CASE REPORT

RJME Romanian Journal of Morphology & Embryology http://www.rjme.ro/

Radiation-associated angiosarcoma of the breast with *MYC* amplification: excisional biopsy–mastectomy correlation in multifocal disease

ZÜLAL SEÇIL IPIN ÇEKIÇ[1)], YELIZ ARMAN KARAKAYA[1)], FERDA BIR[1)], SEVDA YILMAZ[2)], ŞEYMANUR ALA ENLI[3)], PAPATYA BAHAR BALTALARLI[4)], AZIZ GÜLTEKIN[5)]

[1)]*Department of Medical Pathology, Faculty of Medicine, Pamukkale University, Denizli, Türkiye*

[2)]*Department of General Surgery, Faculty of Medicine, Pamukkale University, Denizli, Türkiye*

[3)]*Department of Internal Medicine, Division of Medical Oncology, Faculty of Medicine, Pamukkale University, Denizli, Türkiye*

[4)]*Department of Radiation Oncology, Faculty of Medicine, Pamukkale University, Denizli, Türkiye*

[5)]*Department of Nuclear Medicine, Faculty of Medicine, Pamukkale University, Denizli, Türkiye*

Abstract

Background: Radiation-associated angiosarcoma of the breast (RAASB) is a rare, aggressive late complication of radiotherapy. *Case presentation*: We report a 73-year-old woman who presented with multiple violaceous cutaneous lesions of the right breast 5 years, 11 months, and 2 days after completion of adjuvant radiotherapy for invasive breast carcinoma of no special type. Because lesion onset could not be retrospectively recalled, latency was calculated from radiotherapy completion to clinical evaluation and excisional biopsy on 7 April 2026. Excision of a single 2.0 cm cutaneous lesion established the diagnosis of angiosarcoma. Subsequent total mastectomy demonstrated broader multifocal dermal and subcutaneous involvement and greater histopathological (HP) heterogeneity, including focal solid high-grade growth and tumor necrosis involving 10–15% of the sampled tumor area. Tumor cells expressed vimentin, cluster of differentiation (CD)31, CD34, ETS-related gene (ERG), Friend leukemia integration 1 transcription factor (FLI-1), factor VIII, and D2-40, with strong nuclear c-MYC immunoexpression in >80% of cells. *MYC* fluorescence *in situ* hybridization performed on the mastectomy specimen confirmed high-level amplification, with a MYC/green chromosome 8 centromeric control (SE 8) ratio of 5.06 across 50 tumor nuclei. Surgical margins were tumor-free. At the latest documented follow-up on 21 August 2026, the patient was receiving her ninth cycle of Paclitaxel. Without subsequent imaging, objective disease status remained undetermined. *Discussions*: Comparison of the excisional biopsy and mastectomy specimens showed that a diagnostically adequate biopsy of a single lesion may underrepresent the multifocal extent and HP heterogeneity of RAASB. *Conclusions*: *MYC* analysis provides complementary diagnostic evidence and should be interpreted within the integrated clinicopathological context.

Keywords: radiation-associated angiosarcoma, breast, *MYC* amplification, fluorescence *in situ* hybridization, surgical pathology.

Introduction

Radiation-associated angiosarcoma of the breast (RAASB) is a rare but well-recognized late complication of adjuvant radiotherapy following breast-conserving surgery, representing the most common histopathological (HP) subtype among secondary breast sarcomas [1–3]. Whereas primary breast angiosarcoma predominantly occurs in younger patients, RAASB generally affects older women, with a mean age in the seventh decade of life [1, 4]. Although the tumor typically develops approximately 5–6 years after radiotherapy, the latency period may be as short as 1–2 years in rare cases [5, 6].

Because the clinical findings are non-specific and the lesions may be mistaken for benign dermatological conditions, hematoma, or radiation dermatitis, early diagnosis can be challenging. Lesions typically present as solitary or multiple erythematous or violaceous plaques, papules, or nodules [4, 7]. In most cases, the tumor consists of multifocal, firm, or spongy hemorrhagic masses involving the dermis and subcutaneous adipose tissue, and the true extent of disease may be greater than is clinically or macroscopically apparent [4, 8, 9].

Histopathologically, RAASB is characterized by the proliferation of malignant endothelial cells showing variable degrees of cytological atypia and the formation of irregular, inter-anastomosing vascular channels [2, 10, 11]. *MYC* gene amplification at chromosome 8q24 is a characteristic, but not universal, molecular alteration in secondary angiosarcomas [12–14]. In the appropriate clinicopathological setting, *MYC* amplification by fluorescence *in situ* hybridization (FISH), together with c-MYC immunoexpression, provides complementary evidence in the differential diagnosis from post-radiation atypical vascular lesions (AVLs) [11–14].

Herein, we report a multifocal high-grade RAASB in which complete excision of a single cutaneous lesion established the diagnosis, whereas subsequent mastectomy demonstrated broader multifocal extent and HP heterogeneity. The educational value lies in the biopsy–resection comparison and in the integrated interpretation of morphology, endothelial immunophenotype, and *MYC* amplification.

This is an open-access article distributed under the terms of a Creative Commons Attribution-NonCommercial-ShareAlike 4.0 International Public License, which permits unrestricted use, adaptation, distribution and reproduction in any medium, non-commercially, provided the new creations are licensed under identical terms as the original work and the original work is properly cited.

Materials and Methods

Clinical records, nuclear imaging findings, and archived HP material from the excisional biopsy and total mastectomy were retrospectively reviewed.

Histopathological assessment and tissue sampling

The excisional biopsy consisted of complete removal of a single violaceous cutaneous lesion (measuring 2.0 cm in maximum diameter) from the 9 o'clock region of the right breast and was submitted entirely in one block. The mastectomy specimen was serially sectioned at approximately 1 cm intervals and sampled in 38 cassettes. Approximately half of each grossly visible skin lesion was sampled; the lesion surrounding the previous excision scar was submitted entirely. Fibrotic and tumor-associated areas were sampled across serial slices, together with representative additional areas and surgical margins.

Tissues were fixed in 10% neutral buffered formalin for 24 hours, processed using a Sakura Tissue-Tek VIP 6 AI automated tissue processor, embedded in paraffin, and sectioned at 3 μm. Tumor extent was assessed by correlating gross multifocality with microscopic dermal and subcutaneous infiltration. Because of the multifocal tumor distribution within an extensive fibrotic field, a single continuous microscopic span of infiltration could not be reliably determined. Therefore, the largest gross tumor focus and the dimensions of the overall fibrotic field were documented separately. Tumor necrosis was quantitatively evaluated on sampled sections by its presence and percentage extent (focal necrosis occupying approximately 10–15% of the evaluated tumor field). Mitotic activity was assessed on phosphohistone H3 (pHH3)-stained sections in the most mitotically active area (hotspot) using an Olympus BX53 light microscope equipped with a ×40 objective [total field area corresponding to 10 high-power fields (HPFs): 2.2 mm^2]. pHH3-positive apoptotic nuclei were excluded, and 25 mitoses were counted across 10 HPFs (11.3 mitoses/mm^2).

Immunohistochemistry

Immunohistochemical staining was performed on 3-μm formalin-fixed, paraffin-embedded sections from both the biopsy and mastectomy specimens using the Roche/Ventana BenchMark ULTRA automated staining platform with the OptiView 3,3'-Diaminodenzidine (DAB) immunohistochemistry (IHC) Detection Kit (Ventana Medical Systems, Tucson, AZ, USA). Antigen retrieval was performed using Cell Conditioning 1 [CC1; Tris-Ethylenediaminetetra-acetic acid (EDTA) buffer, pH 8.5] at 95°C for 64 minutes, followed by incubation with ready-to-use primary antibodies at 37°C for 32 minutes.

Mitotic activity was assessed on pHH3-stained sections in the most mitotically active hotspot using an Olympus BX53 light microscope with a ×40 objective. pHH3-positive apoptotic nuclei were excluded. A total of 25 mitoses were counted across 10 HPFs, corresponding to an evaluated area of 2.2 mm^2 and a mitotic density of 11.3 mitoses/mm^2.

External positive controls [appendix for pan-cytokeratin (PanCK) and cluster of differentiation 31 (CD31); tonsil for ETS-related gene (ERG) and c-MYC] were run concurrently. Surrounding non-neoplastic vascular endothelial cells served as internal positive controls for endothelial markers, while non-neoplastic stromal and inflammatory cells provided internal negative reference elements where applicable. No separate negative reagent control was performed. c-MYC expression was evaluated semiquantitatively across the entire tumor area and showed strong nuclear staining in >80% of neoplastic cells. The Ki-67 index was determined by counting tumor cells within a single HPF (×400 magnification) in the proliferative hotspot, with non-neoplastic inflammatory cells strictly excluded. Endothelial markers were evaluated according to their expected cellular localization, staining extent, and intensity. Antibody-specific clones, catalogue numbers, manufacturers, and staining results are provided in Table 1.

Table 1 – ***Complete immunohistochemical panel actually performed in the present case***

Marker	Clone / Catalogue No. / Manufacturer	Tumor cell localization	Extent / intensity	Interpretation
Vimentin	V9 / Cat. No. 790-2917 / Roche (Ventana)	Cytoplasmic	Diffuse / strong	Positive
CD31	JC70A / Cat. No. 760-4378 / Roche (Ventana)	Membranous	Diffuse / strong	Positive
CD34	QBEnd/10 / Cat. No. 790-2927 / Roche (Ventana)	Membranous / cytoplasmic	Diffuse / moderate	Positive
ERG	EPR3864 / Cat. No. 6478813001 / Roche (Ventana)	Nuclear	Diffuse / strong	Positive
FLI-1	MRQ-1 / Cat. No. 760-4384 / Roche (Ventana)	Nuclear	Diffuse / moderate	Positive
Factor VIII	Polyclonal / Cat. No. 760-2642 / Roche (Ventana)	Cytoplasmic	Focal / moderate	Positive
D2-40	D2-40 / Cat. No. 760-4350 / Roche (Ventana)	Membranous	Focal / moderate	Positive
c-MYC	Y69 / Cat. No. 790-4628 / Roche (Ventana)	Nuclear	Diffuse (>80%) / strong	Positive
Ki-67	30-9 / Cat. No. 790-4286 / Roche (Ventana)	Nuclear	Approximately 70% in hotspot	High proliferative index
pHH3	Polyclonal / Cat. No. 760-4591 / Roche (Ventana)	Nuclear in mitotic figures	25 mitoses/10 HPFs (2.2 mm^2); apoptotic nuclei excluded	Mitotic activity assessment
PanCK	AE1/AE3/PCK26 / Cat. No. 760-2135 / Roche (Ventana)	No tumor cell staining	0%; negative	Negative
CK7	SP52 / Cat. No. 790-4462 / Roche (Ventana)	No tumor cell staining	0%; negative	Negative
CK20	SP33 / Cat. No. 790-4431 / Roche (Ventana)	No tumor cell staining	0%; negative	Negative
HMB45	HMB45 / Cat. No. 790-4366 / Roche (Ventana)	No tumor cell staining	0%; negative	Negative
S100	Polyclonal / Cat. No. 760-2523 / Roche (Ventana)	No tumor cell staining	0%; negative	Negative
TRPS1	SP161 / Cat. No. 790-7117 / Roche (Ventana)	No tumor cell staining	0%; negative	Negative
E-cadherin	36 / Cat. No. 790-4497 / Roche (Ventana)	No tumor cell staining	0%; negative	Negative

Marker	Clone / Catalogue No. / Manufacturer	Tumor cell localization	Extent / intensity	Interpretation
p63	4A4 / Cat. No. 790-4509 / Roche (Ventana)	No tumor cell staining	0%; negative	Negative
CD10	SP67 / Cat. No. 790-4506 / Roche (Ventana)	No tumor cell staining	0%; negative	Negative
GCDFP-15	EP1582Y / Cat. No. 760-4381 / Roche (Ventana)	No tumor cell staining	0%; negative	Negative
EMA	E29 / Cat. No. 760-4291 / Roche (Ventana)	No tumor cell staining	0%; negative	Negative
GATA3	L50-823 / Cat. No. 760-4897 / Roche (Ventana)	No tumor cell staining	0%; negative	Negative
HHV8	13B10 / Cat. No. 760-4377 / Roche (Ventana)	No tumor cell staining	0%; negative	Negative
CAMTA1	Polyclonal / Cat. No. bs-12941R / Bioss Antibodies [distributed for Roche (Ventana)]	No tumor cell nuclear staining	0%; negative	Negative
p53	DO-7 / Cat. No. 790-2912 / Roche (Ventana)	Nuclear	Approximately 15%; wild-type pattern	Wild-type pattern

CAMTA1: Calmodulin-binding transcription activator 1; CD: Cluster of differentiation; CK: Cytokeratin; EMA: Epithelial membrane antigen; ERG: ETS-related gene; FLI-1: Friend leukemia integration 1 transcription factor; GATA3: GATA-binding protein 3; GCDFP-15: Gross cystic disease fluid protein-15; HHV8: Human herpesvirus 8; HMB45: Human melanoma black 45; HPF: High-power field; MYC: MYC proto-oncogene; pHH3: Phosphohistone H3; TRPS1: Transcriptional repressor GATA binding 1.

Fluorescence *in situ* hybridization

Dual-color FISH was performed on 4-μm formalin-fixed, paraffin-embedded tissue sections using the Kreatech ON *MYC* (8q24)/green chromosome 8 centromeric control (SE 8) Dual Color FISH Probe [Catalogue No. KBI-10106; Kreatech Biotechnology B.V. (Leica Biosystems), Amsterdam, The Netherlands]. Tissue sections underwent automated deparaffinization, heat pretreatment in 10 mM sodium citrate buffer at 98°C for 15 minutes, and pepsin digestion at 37°C for 10 minutes. Probe co-denaturation was performed at 75°C for 5 minutes, followed by hybridization at 37°C for 16 hours. Post-hybridization stringent washing was performed in 0.4× standard saline citrate (SSC)/0.3% NP-40 at 72°C for 2 minutes, followed by counterstaining with 4',6-Diamidino-2-phenylindole (DAPI).

Fluorescence signals were visualized using single-bandpass filter sets for DAPI (blue nuclear counterstain; excitation 350 nm/emission 460 nm), Fluorescein isothiocyanate (FITC)/Green (SE 8 centromeric signal; excitation 490 nm/emission 520 nm), and Texas Red/Rhodamine (MYC orange-red signal; excitation 570 nm/emission 590 nm), together with a triple-bandpass DAPI/FITC/Texas Red filter set for simultaneous multicolor signal assessment.

Signal visualization, image acquisition, and enumeration were performed using a Leica DM6000 B epifluorescence microscope equipped with a ×63 oil-immersion objective, a JAI CV-M4+ camera, and CytoVision image analysis software (Leica Biosystems). Tumor hotspots were selected by correlation with the corresponding Hematoxylin–Eosin (HE)- and c-MYC-immunostained sections. Two independent observers evaluated 50 intact, non-overlapping tumor nuclei across two spatially distinct fields. Only individually discernible *MYC* and SE 8 signals were included in the quantitative count. Dense *MYC* signal clusters were recorded qualitatively as present but were not assigned a fixed numerical value; only separately resolvable signals contributed to the calculation of the mean signal numbers and *MYC*/SE 8 ratio. *MYC* amplification was defined as a *MYC*/SE 8 ratio ≥2.0, consistent with the published *MYC*/centromere of chromosome 8 (CEP8) FISH criterion [15]. Surrounding non-neoplastic endothelial and stromal cells served as internal diploid controls, showing two *MYC* and two SE 8 signals.

Case presentation

A 73-year-old woman underwent right segmental mastectomy and sentinel lymph node (LN) biopsy on 15 October 2019. The HP diagnosis was established on 19 October 2019 as invasive breast carcinoma of no special type (NST), Nottingham grade 2 (tubule formation 3, nuclear pleomorphism 2, mitotic score 1; total score 6), pT2 pN0(sn) (0/3 LNs). The primary surgery and pathological evaluation were performed at an outside institution; the available external report documented estrogen receptor (ER) 100% (+++), progesterone receptor (PR) 100% (+++), and human epidermal growth factor receptor 2 (HER2) negativity (IHC score 0). Because archival tissue blocks and slides from the primary tumor were unavailable for retrospective review, compliance with specific biomarker scoring guidelines or additional parameters (such as lympho-vascular invasion and Ki-67) could not be independently verified. Adjuvant Doxorubicin and Cyclophosphamide followed by Paclitaxel chemotherapy was administered between 22 November 2019 and 24 January 2020, followed by adjuvant endocrine therapy with Anastrozole. A detailed clinicopathological and therapeutic timeline of the patient is summarized in Table 2.

Table 2 – ***Detailed clinicopathological and therapeutic timeline in the present case***

Date / period	Clinical phase	Key events and details
15 October 2019	Breast-conserving surgery	Right segmental mastectomy and sentinel LN biopsy were performed.
19 October 2019	HP diagnosis	HP examination established the diagnosis of invasive breast carcinoma of NST, Nottingham grade 2 (tubule formation 3, nuclear pleomorphism 2, mitotic score 1; total score 6), pT2 pN0(sn) (0/3 LNs). ER 100% (+++), PR 100% (+++), and HER2 negative (IHC score 0). Surgical margins were tumor-free (closest inferior margin: 3 cm).
22 November 2019–24 January 2020	Systemic chemotherapy	Adjuvant Doxorubicin and Cyclophosphamide followed by Paclitaxel.
9 March 2020–5 May 2020	Adjuvant radiotherapy	Adjuvant radiotherapy for the right breast using 6-MV IMRT on a TomoTherapy platform. The documented total dose was 62 Gy in 31 fractions (2 Gy/fraction). Detailed whole-breast/boost dose allocation, target volumes, dose distribution, and regional nodal irradiation information were unavailable.

Date / period	Clinical phase	Key events and details
25 May 2020–April 2026	Endocrine therapy and latency	Adjuvant Anastrozole therapy. The verified latency interval was 5 years, 11 months, and 2 days, calculated from completion of radiotherapy on 5 May 2020 to the initial clinical evaluation and excisional biopsy on 7 April 2026.
7 April 2026	Initial diagnostic biopsy	Complete excisional biopsy of a single 2-cm violaceous cutaneous nodule in the irradiated right breast. HP examination and IHC established the diagnosis of high-grade RAASB.
15 April 2026	Clinical staging	Whole-body ^{18}F-FDG PET/CT demonstrated multiple hypermetabolic cutaneous and subcutaneous foci confined to the right breast, including a dominant 15.4-mm retroareolar nodule (SUV_{max} 7.13). No regional LN, visceral, osseous, or distant soft-tissue metastases were identified.
18 May 2026	Definitive surgery	Right total mastectomy was performed 41 days after the excisional biopsy. The specimen contained seven cutaneous nodules measuring up to 2 cm and a 4-cm gross tumor focus within a 6×6×4 cm fibrotic field. Surgical margins were tumor-free (closest peripheral margin: 1.5 cm; deep fascial margin: 3.5 cm).
21 August 2026	Most recent follow-up	The patient was receiving her ninth cycle of systemic Paclitaxel chemotherapy. Because no post-treatment imaging assessment was available, current objective disease status could not be definitively determined.

ER: Estrogen receptor; ^{18}F-FDG: Fluorine-18 fluorodeoxyglucose; HER2: Human epidermal growth factor receptor 2; HP: Histopathological; IHC: Immunohistochemistry; IMRT: Intensity-modulated radiotherapy; LN: Lymph node; NST: No special type; PET/CT: Positron emission tomography/computed tomography; PR: Progesterone receptor; RAASB: Radiation-associated angiosarcoma of the breast; SUV_{max}: Maximum standardized uptake value.

Adjuvant radiotherapy for the right breast carcinoma was delivered from 9 March to 5 May 2020 using 6-MV intensity-modulated radiotherapy (IMRT) on a TomoTherapy platform. The available records documented a total dose of 62 Gy in 31 fractions. However, detailed treatment records specifying the whole-breast and potential boost components, target volumes, dose distribution, and regional nodal irradiation were unavailable. Therefore, the relationship of the subsequent angiosarcoma to a specific high-dose subfield could not be retrospectively confirmed, although the lesions arose within the previously irradiated right breast.

The exact date of the first appearance of the cutaneous lesions could not be retrospectively recalled by the patient.

On 7 April 2026, 5 years, 11 months, and 2 days after completion of radiotherapy, the patient was evaluated for newly developed multiple slightly elevated violaceous nodular lesions involving all quadrants of the right breast skin, the largest clinically measuring approximately 2 cm. A single lesion at the 9 o'clock position was completely removed by excisional biopsy on the same date, and HP examination established the diagnosis of angiosarcoma before definitive surgery. Positron emission tomography/computed tomography (PET/CT) imaging performed on 15 April 2026 was acquired on a GE HealthCare digital PET/CT scanner (GE HealthCare, Waukesha, WI, USA) using Q.Clear reconstruction technology. Whole-body fluorine-18 fluorodeoxyglucose (^{18}F-FDG) PET/CT demonstrated multiple FDG-avid lesions confined to the right breast (Figure 1A), without pathological FDG uptake in regional LNs or evidence of visceral, osseous, or distant soft tissue metastasis. Maximum standardized uptake values (SUV_{max}) of the hypermetabolic lesions were quantified by drawing three-dimensional (3D) spherical volumes of interest (VOIs) encompassing the lesions using the AW Server workstation software (GE HealthCare), normalized to total body weight (Figure 1, B–D).

Gross examination of the mastectomy specimen demonstrated seven violaceous nodular cutaneous lesions (largest measuring 2.0 cm; Figure 2A) and multiple dark red-brown hemorrhagic nodules (largest gross focus measuring 4.0 cm; Figure 2, B and C) within a 6×6×4 cm fibrotic field.

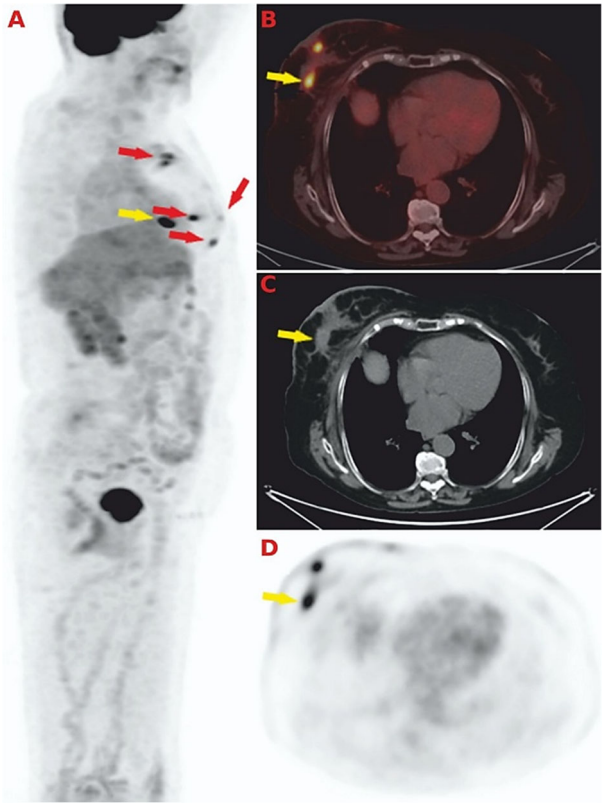

Figure 1 – ***Staging ^{18}F-FDG PET/CT images demonstrating multiple hypermetabolic lesions in the right breast, without regional nodal or distant systemic metastases. (A) Whole-body MIP image showing multiple pathological uptake foci in the right breast. The yellow arrow indicates the dominant retroareolar nodule (15.4 mm; SUV_{max} 7.13), while the red arrows indicate additional cutaneous and subcutaneous nodular foci, including upper-outer-quadrant lesions (SUV_{max} 6.28) and a lower-inner-quadrant nodule (SUV_{max} 4.41). Corresponding axial fused PET/CT (B), axial CT (C), and axial PET (D) images demonstrate the dominant hypermetabolic retroareolar nodule (yellow arrows). The source images were exported directly from the Nuclear Medicine workstation at the maximum available resolution and subsequently arranged and annotated for publication. ^{18}F-FDG: Fluorine-18 fluorodeoxyglucose; MIP: Maximum intensity projection; PET/CT: Positron emission tomography/computed tomography; SUV_{max}: Maximum standardized uptake value.***

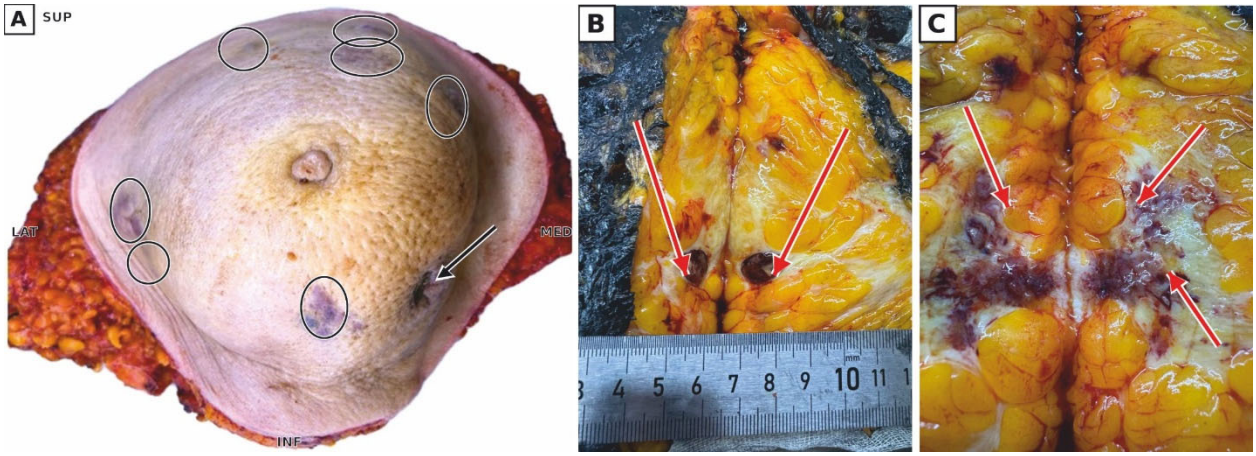

Figure 2 – ***Gross pathological findings of the total mastectomy specimen. (A) External surface of the mastectomy specimen showing seven violaceous nodular and plaque-like cutaneous lesions within the irradiated field (black outlines; largest lesion, 2.0 cm). The arrow indicates the previous biopsy site. Anatomical orientation is indicated as SUP, INF, LAT, and MED. (B) Cut surface showing smaller, discrete dark red-brown hemorrhagic tumor foci (arrows); a metric ruler is shown. (C) Additional cut-surface view demonstrating a broader, irregular area of hemorrhagic tumor involvement (arrows). Across the specimen, the largest gross tumor focus measured 4.0 cm, within an overall fibrotic/tumor-associated field measuring 6×6×4 cm. INF: Inferior; LAT: Lateral; MED: Medial; SUP: Superior.***

Microscopic examination of both the biopsy and mastectomy specimens confirmed an infiltrative malignant endothelial proliferation forming irregular anastomosing vascular channels (Figure 3A), with marked nuclear pleomorphism and prominent extravasated erythrocytes (Figure 3B).

Although the excisional biopsy established the diagnosis (Figure 3, A and B), the mastectomy specimen revealed broader dermal and subcutaneous infiltration. It also demonstrated greater HP heterogeneity, including solid high-grade areas with marked cytological atypia and endothelial tufting (Figure 3C), together with focal tumor necrosis involving approximately 10–15% of the sampled tumor area (Figure 3D).

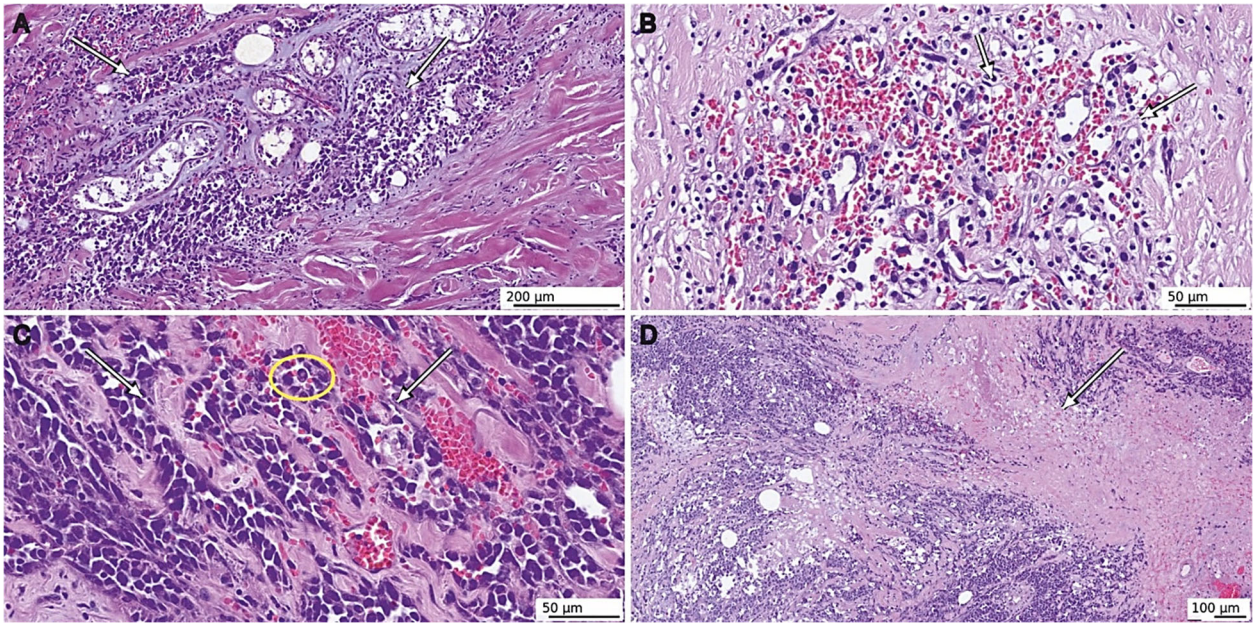

Figure 3 – ***Histopathological comparison between excisional biopsy and total mastectomy specimens: (A) Excisional biopsy specimen demonstrating dermal infiltration by irregular inter-anastomosing vascular channels dissecting collagen (arrows); (B) Excisional biopsy specimen showing prominent extravasated erythrocytes (arrows) and cytological atypia; (C) Total mastectomy specimen demonstrating solid high-grade malignant endothelial proliferation with marked cytological atypia and atypical mitosis (yellow circle); (D) Total mastectomy specimen showing focal tumor necrosis (arrow), occupying approximately 10–15% of the sampled tumor area and surrounded by viable malignant cells. Hematoxylin–Eosin (HE) staining. Scale bar: (A) 200 µm; (B and C) 50 µm; (D) 100 µm.***

Immunohistochemically, tumor cells were positive for vimentin, CD31 (Figure 4A), CD34, ERG (Figure 4B), FLI-1, factor VIII, and D2-40, supporting endothelial differentiation. Strong nuclear c-MYC immunoexpression was present in >80% of cells (Figure 4C). Ki-67 was approximately 70% in the proliferative hotspot (Figure 4D).

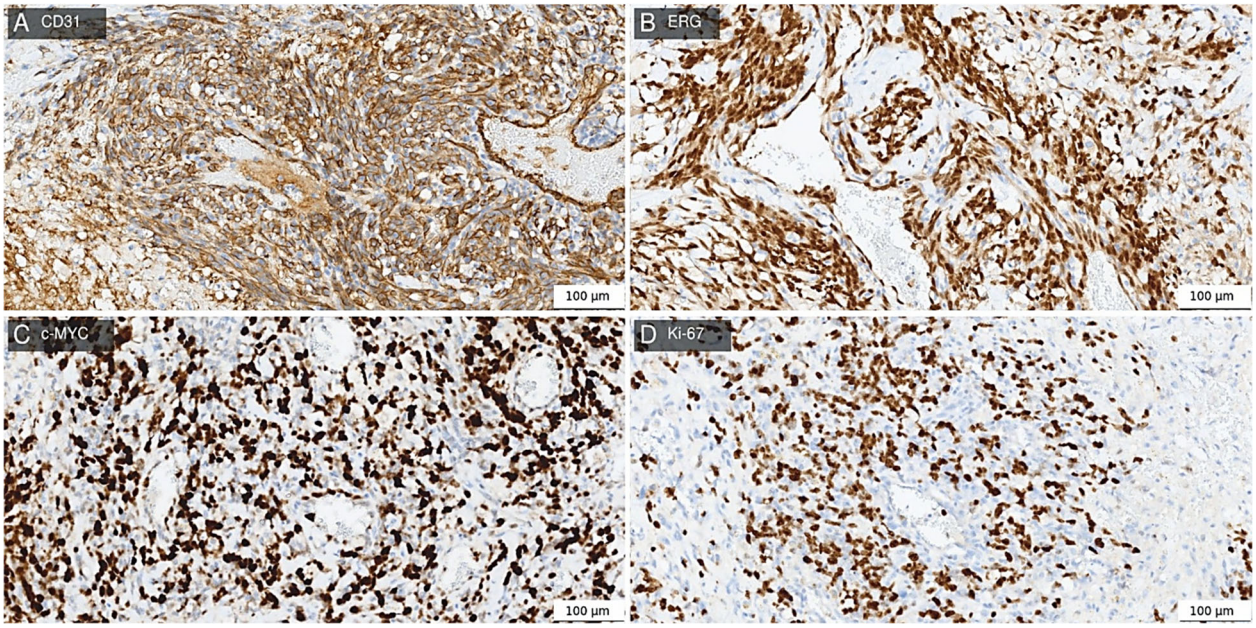

Figure 4 – ***Diagnostic immunohistochemical profile of the tumor: (A) Diffuse, strong membranous reactivity for CD31 in neoplastic endothelial cells forming irregular vascular channels; (B) Strong, diffuse nuclear ERG immunoexpression confirming endothelial differentiation; (C) Diffuse, intense nuclear c-MYC protein expression present in >80% of neoplastic cells; (D) High Ki-67 proliferation index (approximately 70% in hotspot areas), demonstrating brisk tumor cell proliferation. Scale bar: (A–D) 100 µm. CD31: Cluster of differentiation 31; MYC: MYC proto-oncogene; ERG: ETS-related gene.***

The performed negative panel included PanCK, cytokeratin (CK)7, CK20, human melanoma black 45 (HMB45), S100, transcriptional repressor GATA binding 1 (TRPS1), E-cadherin, p63, cluster of differentiation 10 (CD10), gross cystic disease fluid protein-15 (GCDFP-15), epithelial membrane antigen (EMA), GATA-binding protein 3 (GATA3), human herpesvirus 8 (HHV8), and calmodulin-binding transcription activator 1 (CAMTA1). p53 showed an approximately 15% wild-type staining pattern. The absence of epithelial/breast-lineage marker expression, together with the malignant endothelial morphology and endothelial immunophenotype, supported a new vascular malignancy rather than recurrence of the previous breast carcinoma. Mitotic activity assessed on pHH3-stained sections in a hotspot was 25 mitoses/10 HPFs (2.2 mm^2; 11.3 mitoses/mm^2), excluding pHH3-positive apoptotic nuclei. Lymphovascular invasion was not separately assigned as a case variable for the angiosarcoma because of its intrinsically vasoformative malignant endothelial nature. Complete case-specific immunohistochemical results are summarized in Table 1.

MYC FISH was performed on the mastectomy material because of the strong nuclear c-MYC immunoexpression and confirmed high-level gene amplification with a *MYC*/SE 8 ratio of 5.06 across 50 evaluated tumor nuclei (mean 10.12 *MYC* signals and 2.00 SE 8 signals per nucleus) (Figure 5, A and B). Dense *MYC* signal clusters were observed qualitatively in neoplastic cells but were not assigned a fixed numerical value; the reported mean signal numbers and *MYC*/SE 8 ratio were calculated using individually discernible signals. Internal control non-neoplastic stromal cells maintained a normal 1:1 signal ratio (2 *MYC*, 2 SE 8), confirming true *MYC* gene amplification rather than chromosome 8 polysomy. Panels A (Figure 5A) and B (Figure 5B) represent two spatially distinct tumor areas. *MYC* amplification was interpreted as complementary molecular evidence in the context of the radiotherapy history, morphology, and endothelial immunophenotype, rather than as an isolated diagnostic criterion.

Overall, the findings supported a diagnosis of high-grade radiation-associated angiosarcoma of the breast. A formal *Fédération Nationale des Centres de Lutte Contre le Cancer* (FNCLCC) grade was not assigned because of the limitations of applying this grading system to breast/radiation-associated angiosarcoma; instead, the tumor was characterized by its high-grade morphological features, brisk mitotic activity, and necrosis. All mastectomy surgical margins were tumor-free. The minimum distances to the peripheral and deep (fascial) margins were 1.5 cm and 3.5 cm, respectively, and no deep fascial invasion was identified.

At the latest documented follow-up on 21 August 2026, the patient was receiving her ninth cycle of Paclitaxel chemotherapy. Post-treatment follow-up imaging (such as PET/CT) had not yet been performed; therefore, current objective disease status could not be definitively determined.

Discussions

According to the 5th edition of the *World Health Organization (WHO) Classification of Soft Tissue and Bone Tumours*, radiation-associated angiosarcoma is recognized as an aggressive secondary malignant vascular neoplasm requiring rigorous clinicopathological separation from benign post-radiation AVL [16, 17]. Radiation-associated angiosarcoma is diagnosed by integrating the history of prior irradiation, appropriate latency, and anatomical relationship to the treated region with characteristic malignant vascular morphology. Post-radiation AVL is the principal morphological differential diagnosis. In contrast to RAASB, AVLs are generally small, superficial, and relatively circumscribed, with single-layered endothelial channels, minimal atypia, low mitotic activity, and absence of destructive infiltration,

solid growth, or necrosis; *MYC* amplification is generally absent [5, 11, 13, 16]. In this specimen, multifocal infiltrative dermal and subcutaneous growth, marked cytological atypia, brisk mitotic activity (25 mitoses/10 HPFs), solid high-grade areas, focal necrosis, and *MYC* amplification supported angiosarcoma [10–14].

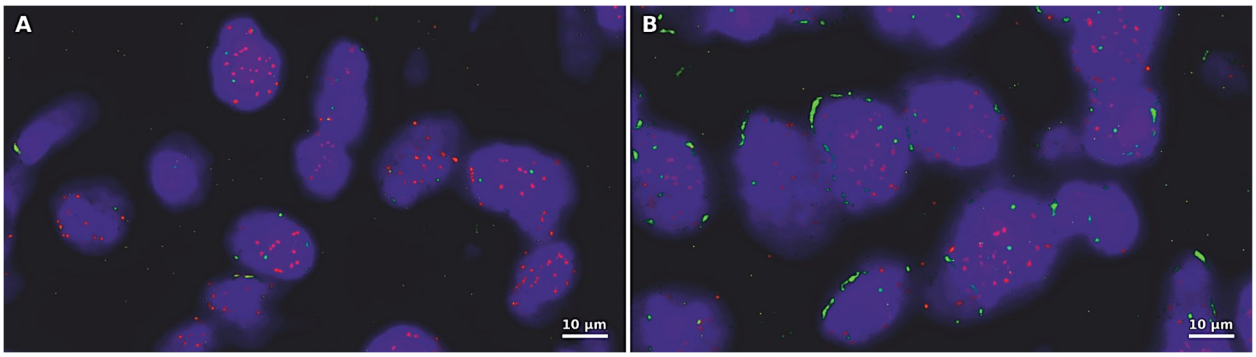

Figure 5 – ***(A and B) MYC amplification detected by dual-color FISH. Representative tumor fields demonstrate numerous orange-red MYC (8q24) signals relative to SE 8 signals in DAPI-counterstained tumor nuclei, consistent with MYC amplification. The Kreatech ON MYC (8q24)/SE 8 Dual Color probe was used. Quantitative assessment of 50 tumor nuclei from two spatially distinct areas yielded a mean of 10.12 MYC signals and 2.00 SE 8 signals per nucleus, corresponding to a MYC/SE 8 ratio of 5.06. (Non-neoplastic endothelial and stromal cells showing the expected disomic signal pattern served as internal controls). Scale bar: (A and B) 10 µm. DAPI: 4',6-Diamidino-2-phenylindole; FISH: Fluorescence in situ hybridization; MYC: MYC proto-oncogene; SE 8: Green chromosome 8 centromeric control.***

MYC amplification is strongly associated with secondary angiosarcoma but is not universal and should not replace morphological assessment [12–14]. Mentzel *et al.* demonstrated *MYC* amplification in post-radiation cutaneous angiosarcomas but not in AVL in their cohort [13], while Kuba *et al.* identified amplification in 73 of 81 radiation-associated breast angiosarcomas [14]. Accordingly, c-MYC immunoexpression and *MYC* gene amplification should be distinguished: protein expression is not a perfect surrogate for gene-level amplification, and both findings require clinico-pathological correlation [12–14]. A focused differential diagnosis comparing RAASB with other cutaneous and vascular mimics is summarized in Table 3.

Table 3 – ***Focused differential diagnosis of radiation-associated angiosarcoma of the breast***

Differential diagnosis	Key clinical / morphological features	Typical IHC / molecular features	Findings in present case
Post-radiation AVL	Usually small, superficial dermal and relatively circumscribed; single-layered endothelial channels; minimal atypia; low mitotic activity; no destructive infiltration, solid growth or necrosis.	CD31/ERG positive; *MYC* amplification generally absent.	Multifocal infiltrative dermal/subcutaneous growth, marked atypia, brisk mitotic activity, solid growth and necrosis; *MYC* amplification present.
Kaposi sarcoma	Slit-like vascular spaces and spindle-cell proliferation with erythrocyte extravasation.	HHV8 positive.	HHV8 negative; marked high-grade endothelial atypia and destructive infiltration.
Recurrent breast carcinoma/epithelial malignancy	Epithelial or gland-forming morphology rather than vasoformative channels.	CKs and/or GATA3 typically positive.	PanCK, CK7 and GATA3 negative; endothelial markers positive.
Melanoma	Epithelioid/spindle-cell proliferation; pigment may be present.	S100, SOX10 and/or melanocytic markers positive.	S100 and HMB45 negative; morphology and endothelial immunophenotype support vascular differentiation.
PASH	Benign stromal proliferation with pseudovascular slit-like spaces; no destructive vascular infiltration.	CD34 often positive; CD31 and ERG negative in stromal cells.	True malignant endothelial vasoformation with CD31/ERG positivity and infiltrative growth.
Benign hemangioma	Well-circumscribed benign vascular proliferation without significant atypia or destructive infiltration.	Endothelial markers positive; *MYC* amplification not expected.	Marked atypia, brisk proliferation, infiltrative growth, necrosis and *MYC* amplification.

AVL: Atypical vascular lesion; CD: Cluster of differentiation; CK: Cytokeratin; ERG: ETS-related gene; GATA3: GATA-binding protein 3; HHV8: Human herpesvirus 8; HMB45: Human melanoma black 45; IHC: Immunohistochemistry; MYC: MYC proto-oncogene; PASH: Pseudoangiomatous stromal hyperplasia; SOX10: Sex determining region Y (SRY)-box transcription factor 10.

The biopsy–resection comparison is the principal educational feature of this case. Complete excision of a single cutaneous lesion (2.0 cm) was sufficient to establish the diagnosis of angiosarcoma; therefore, this was not a missed or misleading biopsy diagnosis. Nevertheless, the subsequent mastectomy revealed a substantially broader multifocal disease field and additional histological heterogeneity, including solid high-grade areas and focal necrosis (10–15%). This distinction is clinically relevant because the true extent of RAASB may exceed that represented by a single sampled lesion [4, 8, 9].

The clinicopathological profile is otherwise within the recognized spectrum of RAASB. In an international multi-center analysis of 53 patients, the median age at diagnosis was 72 years, the median interval between radiotherapy and RAASB diagnosis was 78 months, and the median radiation dose was 57.6 Gy; local recurrence occurred in 43% [18]. A systematic review similarly documented the

tendency of RAASB to occur several years after breast irradiation in older women [19]. The verified latency in our patient was 5 years, 11 months, and 2 days from radiotherapy completion to initial clinical evaluation and diagnostic biopsy (7 April 2026) [1, 5, 18].

Surgical resection with negative margins remains the mainstay of treatment for localized RAASB, whereas the role of systemic therapy depends on disease extent and clinical context [3, 9, 19, 20]. In our patient, total mastectomy achieved tumor-free peripheral and deep margins. At the latest documented follow-up on 21 August 2026, systemic Paclitaxel treatment was ongoing. Because no subsequent objective imaging assessment was available, the present report does not draw conclusions regarding durable disease control or prognosis [1, 18, 19].

Conclusions

Radiation-associated angiosarcoma should be considered when new vascular-appearing cutaneous lesions arise in a previously irradiated breast. Adequate sampling is important because examination of a single lesion, even when diagnostically sufficient, may underrepresent multifocal tumor extent and histological heterogeneity. Integration of radiotherapy history, characteristic morphology, and endothelial immunophenotyping is fundamental for diagnosis, while demonstration of *MYC* amplification may provide valuable complementary evidence in challenging post-radiation vascular lesions.

Conflict of interests

The authors declare that they have no conflict of interests.

Funding

This study was not funded externally.

Ethical approval and consent

Written informed consent was obtained from the patient for publication of this case report, including clinical/pathological data and accompanying images. In accordance with Pamukkale University institutional regulations, single-patient anonymized case reports are exempt from formal Ethics Committee approval. This exemption is specified in the institutional guidelines; however, no formal exemption number was issued to the authors. The study complied with the principles of the Declaration of Helsinki.

Author contributions

Zülal Seçil Ipin Çekiç: conceptualization, investigation, data curation, literature review, writing – original draft; Yeliz Arman Karakaya: histopathological and immunohistochemical evaluation, diagnostic assessment, evaluation/interpretation of FISH analysis, writing – review and editing; Ferda Bir: histopathological evaluation, diagnostic review, supervision, writing – review and editing; Sevda Yilmaz: surgical management, clinical data acquisition, clinical assessment; Şeymanur Ala Enli: clinical data acquisition, oncological assessment; Papatya Bahar Baltalarli: evaluation and interpretation of radiotherapy history and treatment details; Aziz Gültekin: evaluation and interpretation of PET/CT findings and nuclear medicine imaging.

References

[1] Dogan A, Kern P, Schultheis B, Häusler G, Rezniczek GA, Tempfer CB. Radiogenic angiosarcoma of the breast: case report and systematic review of the literature. BMC Cancer, 2018, 18(1):463. https://doi.org/10.1186/s12885-018-4369-7 PMID: 29690864 PMCID: PMC5916720

[2] Billings SD, McKenney JK, Folpe AL, Hardacre MC, Weiss SW. Cutaneous angiosarcoma following breast-conserving surgery and radiation: an analysis of 27 cases. Am J Surg Pathol, 2004, 28(6):781–788. https://doi.org/10.1097/01.PAS.0000126055.33916.0b PMID: 15166670

[3] Banks J, George J, Potter S, Gardiner MD, Ives C, Shaaban AM, Singh J, Sherriff J, Hallissey MT, Horgan K, Harnett A, Desai A, Ferguson DJ, Tillett R, Izadi D, Sadideen H, Jain A, Gerrand C, Holcombe C, Hayes A, Teoh V, Wyld L; Breast Angiosarcoma Surveillance Study (BRASS) collaborative. Breast Angiosarcoma Surveillance Study: UK national audit of management and outcomes of angiosarcoma of the breast and chest wall. Br J Surg, 2021, 108(4):388–394. https://doi.org/10.1093/bjs/znaa128 PMID: 33749771

[4] Jackson KM, Grumley JG. Radiation-induced breast angiosarcoma: updates on a rare disease. Curr Breast Cancer Rep, 2024, 16(2):177–184. https://doi.org/10.1007/s12609-024-00542-5

[5] Brenn T, Fletcher CDM. Radiation-associated cutaneous atypical vascular lesions and angiosarcoma: clinicopathologic analysis of 42 cases. Am J Surg Pathol, 2005, 29(8):983–996. https://doi.org/10.1097/01.PAS.0000156664.04955.83 PMID: 16006792

[6] Yap J, Chuba PJ, Thomas R, Aref A, Lucas D, Severson RK, Hamre M. Sarcoma as a second malignancy after treatment for breast cancer. Int J Radiat Oncol Biol Phys, 2002, 52(5):1231–1237. https://doi.org/10.1016/s0360-3016(01)02799-7 PMID: 11955733

[7] Kirova YM, Vilcoq JR, Asselain B, Sastre-Garau X, Fourquet A. Radiation-induced sarcomas after radiotherapy for breast carcinoma: a large-scale single-institution review. Cancer, 2005, 104(4):856–863. https://doi.org/10.1002/cncr.21223 PMID: 15981282

[8] Abdou Y, Elkhanany A, Attwood K, Ji W, Takabe K, Opyrchal M. Primary and secondary breast angiosarcoma: single center report and a meta-analysis. Breast Cancer Res Treat, 2019, 178(3):523–533. https://doi.org/10.1007/s10549-019-05432-4 PMID: 31522347 PMCID: PMC6817750

[9] Salminen SH, Wiklund T, Sampo MM, Tarkkanen M, Pulliainen L, Böhling TO, Tukiainen E, Hukkinen K, Blomqvist CP. Treatment and prognosis of radiation-associated breast angiosarcoma in a nationwide population. Ann Surg Oncol, 2020, 27(4):1002–1010. https://doi.org/10.1245/s10434-019-08085-1 PMID: 31773514 PMCID: PMC7060227

[10] Zhang H, Turner BM, Katerji H, Hicks DG, Wang X. Vascular lesions of the breast: essential pathologic features and diagnostic pitfalls. Hum Pathol Rep, 2021, 26:300570. https://doi.org/10.1016/j.hpr.2021.300570

[11] Rutland CD, Bean GR, Charville GW. Contemporary diagnostic approach to atypical vascular lesion and angiosarcoma. Semin Diagn Pathol, 2023, 40(4):284–294. https://doi.org/10.1053/j.semdp.2023.04.017 PMID: 37121782

[12] Manner J, Radlwimmer B, Hohenberger P, Mössinger K, Küffer S, Sauer C, Belharazem D, Zettl A, Coindre JM, Hallermann C, Hartmann JT, Katenkamp D, Katenkamp K, Schöffski P, Sciot R, Wozniak A, Lichter P, Marx A, Ströbel P. *MYC* high level gene amplification is a distinctive feature of angiosarcomas after irradiation or chronic lymphedema. Am J Pathol, 2010, 176(1):34–39. https://doi.org/10.2353/ajpath.2010.090637 PMID: 20008140 PMCID: PMC2797867

[13] Mentzel T, Schildhaus HU, Palmedo G, Büttner R, Kutzner H. Postradiation cutaneous angiosarcoma after treatment of breast carcinoma is characterized by *MYC* amplification in contrast to atypical vascular lesions after radiotherapy and control cases: clinicopathological, immunohistochemical and molecular analysis of 66 cases. Mod Pathol, 2012, 25(1):75–85. https://doi.org/10.1038/modpathol.2011.134 PMID: 21909081

[14] Kuba MG, Xu B, D'Angelo SP, Rosenbaum E, Plitas G, Ross DS, Brogi E, Antonescu CR. The impact of *MYC* gene amplification on the clinicopathological features and prognosis of radiation-associated angiosarcomas of the breast. Histopathology, 2021, 79(5):836–846. https://doi.org/10.1111/his.14433 PMID: 34165212 PMCID: PMC8678905

[15] Fernandez AP, Sun Y, Tubbs RR, Goldblum JR, Billings SD. FISH for *MYC* amplification and anti-*MYC* immunohistochemistry: useful diagnostic tools in the assessment of secondary angio-

sarcoma and atypical vascular proliferations. J Cutan Pathol, 2012, 39(2):234–242. https://doi.org/10.1111/j.1600-0560.2011.01843.x PMID: 22121953

[16] World Health Organization (WHO) Classification of Tumours Editorial Board. Breast tumours. 5th edition, vol. 2, WHO Classification of Tumours Series, International Agency for Research on Cancer (IARC) Press, Lyon, France, 2019. https://www.iarc.who.int/news-events/who-classification-of-tumours-5th-edition-volume-2-breast-tumours/

[17] World Health Organization (WHO) Classification of Tumours Editorial Board. Soft tissue and bone tumours. 5th edition, vol. 3, WHO Classification of Tumours Series, International Agency for Research on Cancer (IARC) Press, Lyon, France, 2020. https://publications.iarc.who.int/Book-And-Report-Series/Who-Classification-Of-Tumours/Soft-Tissue-And-Bone-Tumours-2020

[18] Mergancová J, Lierová A, Coufal O, Žatecký J, Melichar B, Zedníková I, Mergancová J, Jesenková A, Šťastný K, Gatěk J, Kubala O, Prokop J, Dyttert D, Karaba M, Schwarzbacherová I, Humeňanská A, Šuk J, Valenta M, Moucha V, Sákra L, Hlávka A, Hácová M, Vojtíšek R, Sochor M, Jirásek T, Zábojníková M, Zemanová M, Macháleková K, Rusnáková D, Kúdelová E, Smolár M. Radiation-associated angiosarcoma of the breast: an international multicenter analysis. Surg Oncol, 2022, 41: 101726. https://doi.org/10.1016/j.suronc.2022.101726 PMID: 35203019

[19] Depla AL, Scharloo-Karels CH, de Jong MAA, Oldenborg S, Kolff MW, Oei SB, van Coevorden F, van Rhoon GC, Baartman EA, Scholten RJ, Crezee J, van Tienhoven G. Treatment and prognostic factors of radiation-associated angiosarcoma (RAAS) after primary breast cancer: a systematic review. Eur J Cancer, 2014, 50(10):1779–1788. https://doi.org/10.1016/j.ejca.2014.03.002 PMID: 24731859

[20] Torres KE, Ravi V, Kin K, Yi M, Guadagnolo BA, May CD, Arun BK, Hunt KK, Lam R, Lahat G, Hoffman A, Cormier JN, Feig BW, Lazar AJ, Lev D, Pollock RE. Long-term outcomes in patients with radiation-associated angiosarcomas of the breast following surgery and radiotherapy for breast cancer. Ann Surg Oncol, 2013, 20(4):1267–1274. https://doi.org/10.1245/s10434-012-2755-y PMID: 23224828 PMCID: PMC5036516

Corresponding author

Zülal Seçil Ipin Çekiç, Research Assistant, MD, Department of Medical Pathology, Faculty of Medicine, Pamukkale University, New Education Building, 2nd Floor, adjacent to the Congress and Culture Centre, Kınıklı Campus, 20070 Denizli, Türkiye; Phone +90 258 296 16 02, Fax +90 258 296 17 65, e-mail: zsecil98@gmail.com

Received: September 12, 2026

Accepted: October 11, 2026